Community-Oriented Data Integration and Communication Framework for Streamflow Forecast Models and Flood Inundation Map Products

Kento Sugiyama[1,2], Carlos Erazo Ramirez[3,4], Ibrahim Demir[3,4]

[1] College of Liberal Arts and Sciences, University of Iowa, Iowa City, IA
[2] West High School, Iowa City, IA
[3] River-Coastal Science and Engineering, Tulane University, New Orleans, LA
[4] ByWater Institute, Tulane University, New Orleans, LA

Abstract

Access to critical flood risk information is often limited by expert-driven workflows that require specialized software, creating a barrier to stakeholder engagement and effective science communication. This study presents a generalized web-based framework that integrates federal datasets to support real-time, scenario-based flood forecasting and mapping across the continental United States. By leveraging state-of-the-art client-side technologies, including WebAssembly, Web Workers, and IndexedDB, we developed an on-demand geoprocessing framework that generates flood inundation maps directly in the browser. Flood maps can be generated from National Water Model forecast outputs and Office of Water Prediction Flood Inundation Mapping products. The framework also provides FEMA Hazus damage assessment capabilities applied to property data from the National Structure Inventory. The platform's capabilities are demonstrated through a case study of the 2019 Midwestern floods, showcasing its value as an accessible and scalable tool for emergency managers, planners, and communities to assess flood risks.

Keywords: flood maps, flood forecasting, web framework, real-time mapping, damage estimation

Software and Data Availability

Software	HyMES-FIM
Developer	Kento Sugiyama
Contact Information	cerazoramirez@tulane.edu
First Available	2025
Programming Language	HTML, CSS, JS, WebAssembly
Cost	Free
Software Availability	https://hydroinformatics.tulane.edu/lab/hymes-fim

This manuscript is an EarthArXiv preprint and has been submitted for possible publication in a peer reviewed journal. Please note this update has been peer-reviewed and is currently undergoing peer review for the second time. Subsequent versions of this manuscript may have slightly different content.

1. Introduction

Flooding is among the most damaging and prevalent natural hazards, resulting in significant economic and infrastructure losses worldwide. In the United States, flood-related damage amounts to tens of billions of dollars annually (Wing et al., 2018) and is likely to increase as extreme weather events become more frequent (Seneviratne et al., 2021; Trenberth et al., 2015). At the same time, ongoing urban expansion further concentrates people and assets in flood-prone areas, thereby increasing risks to human life (IPCC, 2023).

Effective flood mitigation and response are built upon a foundation of robust hydrological modeling, which is essential for understanding and predicting the complex interactions between water and the landscape (Cikmaz et al., 2023; Teng et al., 2017). Modern flood analysis integrates a variety of geospatial datasets to link physical processes with spatial contexts. Digital Elevation Models (DEMs) provide the fundamental topographic data for delineating watersheds and flow paths. Hydrographic datasets, such as the National Hydrography Dataset Plus (NHDPlus), provide a detailed representation of the nation's stream network. Tools such as GDAL (Geospatial Data Abstraction Library) are crucial for transforming these geospatial datasets in preparation for subsequent analyses (Brakebill et al., 2020; Gesch et al., 2002; Moore et al., 2019).

Traditionally, these processes rely on powerful desktop software and tools, such as HEC-RAS, ArcGIS, and QGIS, which enable detailed hydraulic simulations but often require significant computational resources and expertise (Qian et al., 2024; Samela et al., 2018; Tsegaye et al., 2024). More recently, a computationally efficient methodology called Height Above Nearest Drainage (HAND) has gained popularity for large-scale flood inundation mapping (FIM) using moderate-to-coarse-resolution elevation data, typically 10 meters or more (Li et al., 2023; Nobre et al., 2011). By leveraging a relative elevation model framework that quantifies the vertical distance from the nearest drainage channel, HAND can achieve accuracy comparable to traditional methods but with a significantly lower computational cost, making it highly suitable for rapid, scenario-based assessments (Aristizabal et al., 2024; Baruah et al., 2025a; Johnson et al., 2019; NOAA Office of Water Prediction, 2025). In addition, the development of analysis-ready datasets from the National Oceanic and Atmospheric Administration (NOAA) National Water Center (NWC) presents a significant opportunity to advance flood map generation using this computationally efficient HAND approach.

Despite these advances, the practice of flood risk assessment remains constrained by expert-driven workflows and specialized software, creating a significant barrier that limits access to critical flood risk information for non-technical stakeholders, such as emergency managers, urban planners, and community members. In response, a variety of web-based platforms have emerged to democratize access to water resources data and modeling tools. Platforms such as the Iowa Flood Information System (Demir & Krajewski, 2013), National Water Prediction Service (water.noaa.gov), and frameworks for urban flood analysis (Alabbad et al., 2023, 2024; Sufi et al., 2025) provide valuable web-based decision-support tools. On a larger scale, platforms such as Google Earth Engine, Tethys, and CUAHSI HydroShare utilize open-source cloud infrastructure to provide access to vast geospatial datasets and models (DeVries et al., 2020; Gorelick et al.,

2017; Hales et al., 2022; Horsburgh et al., 2015; Nelson et al., 2019). However, these powerful platforms often rely on substantial server-side infrastructure, which can lead to high computational costs, data transfer fees, and a reliance on persistent internet connectivity.

A promising alternative is to explore client-side technologies that enable direct hydrologic analysis in the user's web browser (Sit et al., 2021). Foundational work demonstrating this potential includes the development of the Hillslope Link Model (HLM), a rainfall-runoff simulation engine written in JavaScript (Ewing et al., 2022). This client-side model supports hydrological education and research. Interactive gaming engines (Demiray et al., 2025; Emiroglu et al., 2025) also showcase advanced visualization techniques and analytics in a standard web browser. More recent advances in client-side technologies, such as WebAssembly, WebGPU, and Web Workers, have enabled even more complex analyses. Sit et al. (2019) developed a client-side watershed delineation algorithm using JavaScript, WebAssembly, and WebGL.

The HydroLang framework (Erazo Ramirez et al., 2022, 2023) further advanced this paradigm by providing a comprehensive suite of tools and declarative interfaces for client-side hydrological analysis. In addition, libraries such as HydroCompute (Ramirez et al., 2024) have demonstrated the power of this approach for hydrological computations, achieving performance comparable to that of desktop applications. Additionally, work by Hu and Demir (2021) on client-side flood inundation mapping established the feasibility of real-time flood modeling in the browser by compiling a C++ implementation of the HAND algorithm to WebAssembly. Li and Demir (2022) later developed a comprehensive platform based on this methodology, which included tools for generating custom maps and conducting analyses. These studies demonstrated the technical feasibility of client-side geospatial processing and flood modeling.

However, existing studies have not leveraged client-side technologies to build an operational platform that fully integrates national-scale datasets with forecast models to enable reliable, scenario-based flood inundation mapping across the continental United States. Therefore, this study addresses this gap by developing a web-based platform that leverages client-side processing for real-time flood inundation mapping. Our approach connects the NOAA Office of Water Prediction (OWP) high-quality relative elevation models with discharge predictions from the National Water Model (NWM), enabling reliable, on-demand inundation mapping for any river reach in the continental United States. By building on a nationally consistent hydrofabric (Blodgett & Johnson, 2025), this platform provides emergency managers, planners, and community stakeholders with immediate and intuitive access to flood modeling capabilities. In this paper, we (1) present the client-side architecture for integrating heterogeneous federal datasets; (2) demonstrate its capabilities for real-time, scenario-based flood modeling and infrastructure impact assessment; and (3) evaluate the platform's accuracy and performance through a case study of the 2019 Midwestern floods.

2. Scenario-Based Flood Inundation Mapping Framework

2.1. System Overview

This framework combines interactive flood scenario creation, historical and forecast model outputs, and real-time infrastructure damage estimates into a single, unified user interface. By integrating diverse federal datasets, the system addresses common issues of data fragmentation and accessibility, enabling comprehensive flood inundation mapping and impact analysis within one platform (Table S1 in the supplementary material). The platform initially displays watershed features at various levels, from HUC-2 to HUC-12. Users can generate flood inundation maps at the river-reach level by adjusting stage values directly or by utilizing real-time and retrospective outputs from the National Water Model (NWM). A technical overview of the platform, including web technologies, data sources, and analysis tools, is shown in Figure 1. The analysis features, scenario-based flood extents, and infrastructure assessment are detailed in Section 3.

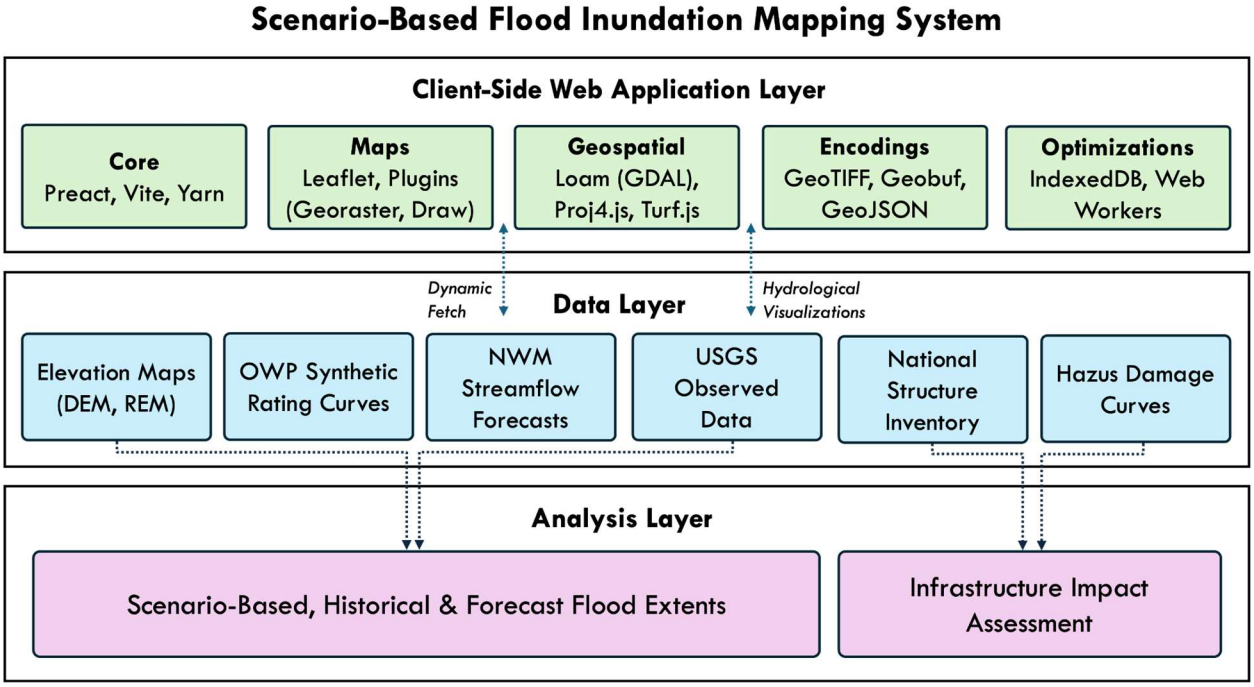

Figure 1. Technical overview and components of the framework.

The platform is built on a modern front-end architecture using Preact and the Vite build tool for optimal performance, with Tailwind CSS for consistent styling (Miller, 2025; Wathan, 2024; You, 2025). This ensures high accessibility and performance across all modern web browsers. The application is primarily driven by user interaction with the mapping engine, providing real-time updates through visualization of diverse data types. Interactive mapping is implemented using the Leaflet library (Agafonkin, 2023), with a simple base map (CARTO, 2024) and specialized layers for visualizing hydrological data. Leaflet was chosen due to its open-source nature and extensibility through community-driven packages and implementations. The system renders raster data using a custom Leaflet GridLayer canvas pipeline with pixel-to-color mapping for elevation

and flood depth. The Leaflet mapping architecture supports diverse visualization requirements, including point-based markers for USGS gauge stations, real-time flood inundation raster overlays, and integrated search functionality with spatial context awareness.

The platform operates on an entirely client-side computing architecture, ensuring high performance and a responsive user interface, without relying on server-side computational resources. The system uses Web Workers to manage asynchronous operations, preventing the main thread from freezing during intensive calculations. For efficient data management, large geospatial datasets and user-generated scenarios are cached locally in the browser using IndexedDB. A detailed description of this processing architecture, including its implementation with WebAssembly for geospatial operations, is provided in Section 3.2. Figure 2 illustrates the technical workflow, shown as a sequence diagram, from initial data preparation through flood mapping and damage assessment.

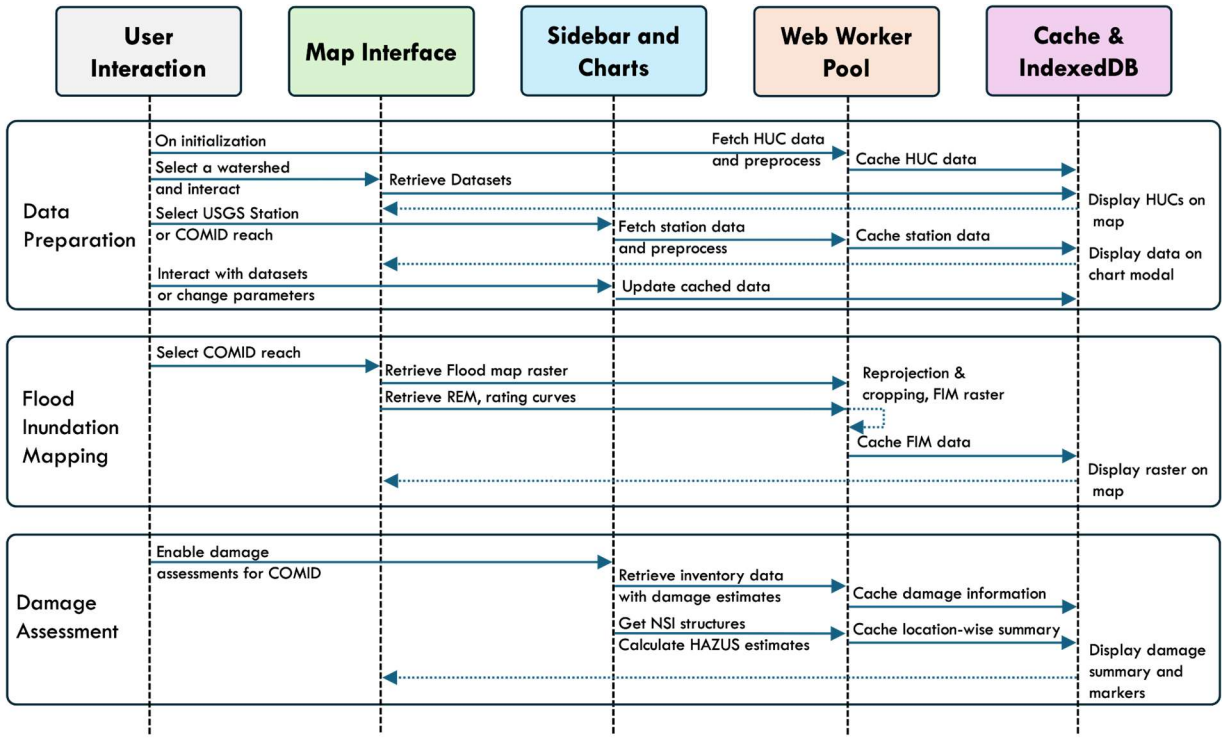

Figure 2. System workflow sequence describing the data flow and processing steps from initial data preparation to flood mapping and damage assessment.

2.2. Hydrological Features and Data Visualization for Analysis

The application displays watersheds by linking them through their respective HUC identifiers, as explained in Jones et al. (2009), using the Watershed Boundary Dataset (WBD). The platform allows for hierarchical watershed views spanning from HUC-2 to HUC-12 levels. HUC-2 catchments for the continental U.S. are initially displayed, with finer HUC levels progressively loaded upon user interaction (Figure 3). The data for HUC-2 and HUC-4 are stored as a single GeoJSON for the continental United States, encoded into the GeoBuf format for compression

(Agafonkin, 2020). For other HUC levels, the USGS Web Feature Service (WFS) server is used to obtain the vector data, enabling fast catchment loading upon request. To aid in visualization, the current HUC level is displayed as a concatenated string in the interface, allowing users to track their navigation through the nested watershed hierarchy.

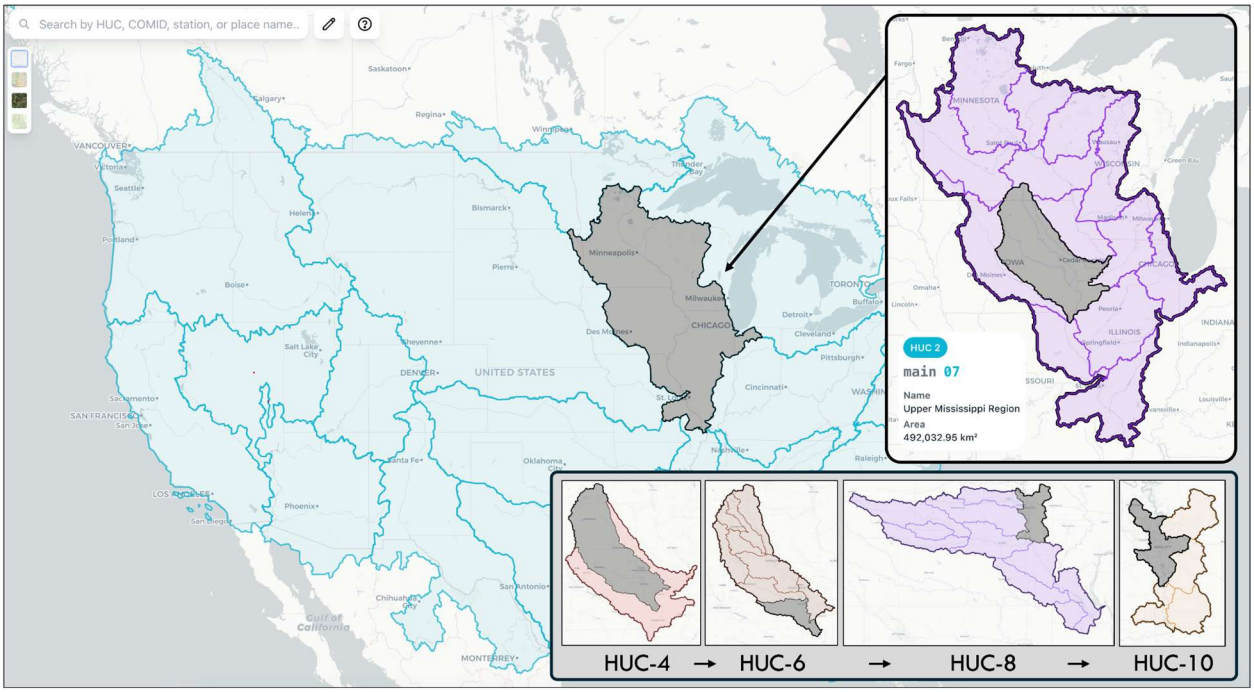

Figure 3. Example interaction of HUC-2 catchments and their corresponding subcatchments across the United States. The inset panel displays the interaction between the higher-order catchments and their children. When a HUC-2 is selected, a panel shows the current HUC level and basic properties about the watershed.

Hydrological features are displayed as layers on the Leaflet basemap (Figure 4). At this zoom level, NHDPlus flowlines and catchments (Brakebill et al., 2020), digital elevation maps (Sugarbaker et al., 2014), and USGS gauge stations (McCallum & Riskin, 2025) are made available. The sidebar includes a FIM preparation section that tracks the retrieved Relative Elevation Model (REM) raster datasets and rating curves stored in the application database at the HUC-8 level. The platform uses preprocessed HAND-based products distributed through a public CIROH cloud mirror of OWP-FIM products.

USGS stations provide observed data used to generate scenario-based flood inundation maps. Upon clicking a station, a modal with metadata panels appears, containing station information, status, historic crests, and flood-related data. In addition to observed USGS discharge, 30-day discharge records were obtained through the National Water Prediction Service (NWPS) web service (Cosgrove et al., 2024). It is worth noting that data availability differs across gauge stations, with variations in record length, continuity, and measurement frequency. Users can also export time-series data through the modal interface.

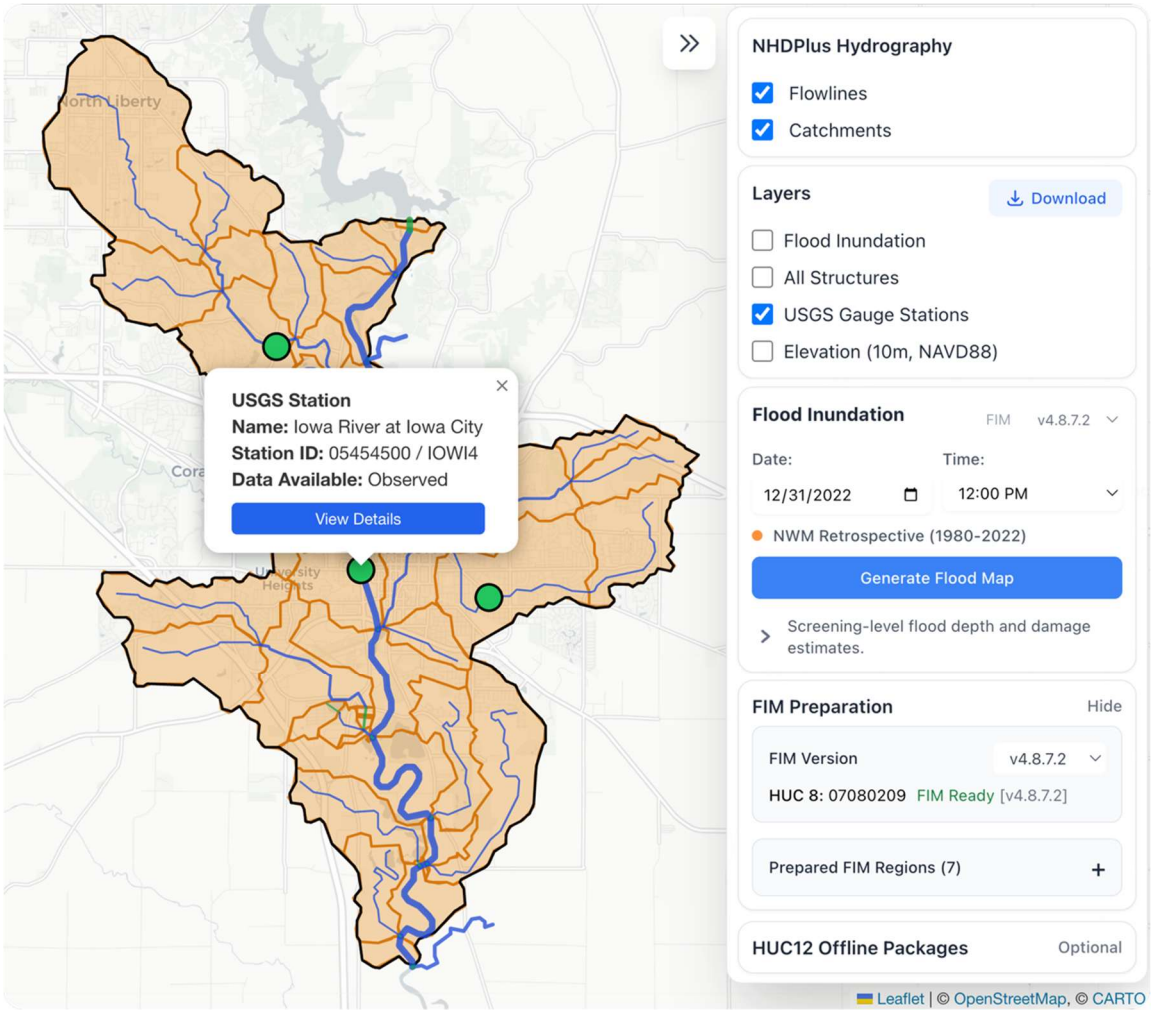

Figure 4. HUC-12 interface showing hydrological layers and flood mapping controls within the platform. The main map displays NHDPlus flowlines and catchments together with USGS gauge stations. The sidebar includes layer toggles, a flood mapping interface, and a FIM preparation panel showing the selected OWP-FIM version, HUC-8 preparation status, and available prepared regions.

At the HUC-12 level, users can select individual river reaches to display reach-specific information using a Common Identifier (COMID) code linked to the National Hydrography Dataset (Brakebill et al., 2020). When selected, the reach displays metadata, including stream names, lengths, stream orders, and drainage areas. Flowline selection provides access to time-series data, along with elevation and flood maps, via specific layers in the sidebar.

For each reach, streamflow prediction data are provided by two complementary National Water Model (NWM) data sources. Historical discharge is obtained from the NWM retrospective dataset (Cosgrove et al., 2024), which provides data from 1980 to 2022, and real-time forecasts are obtained through the National Water Prediction Service (NWPS) API. NWPS provides reach products by forecast time series: analysis assimilation (representing observation-constrained near-

current conditions) and forecasts at short (24-hour), medium (10-day), and long (30-day) time scales. Figure 5 showcases the NWM retrospective display for a river reach in Iowa City, IA, during the 2008 Iowa Floods.

Figure 5. NWM retrospective display for a river reach (COMID: 11916315) in Iowa City, IA, during the 2008 Iowa Floods.

3. Client-Side Processing Architecture

Within the flowline view, users can generate scenario-based maps using the Height Above Nearest Drainage (HAND) methodology (Nobre et al., 2011). This method uses relative elevation models (REMs) and synthetic rating curves derived from catchment-specific hydraulic properties (Baruah et al., 2025b; NOAA Office of Water Prediction, 2025) to produce flood-depth maps at the individual river-reach (COMID) level. Within the platform, user-specified or model-derived discharge values are converted to stage through synthetic rating curves, and these stage values are applied to relative elevation models to generate scenario-based flood inundation maps (Johnson et al., 2019; Thalakkottukara et al., 2024).

3.1. HAND Model Implementation

The platform implements the HAND approach through a multi-branch REM organization at the HUC-8 watershed scale. Following the OWP-FIM framework, the stream network within each HUC-8 is partitioned into continuous level paths (LPs) to reduce spurious influences from neighboring tributaries. The mainstem LP is indexed as branch 0, and tributary LPs are numbered sequentially (Aristizabal et al., 2023).

The HAND method relies on a sequence of geospatial processing steps that transform a hydroconditioned digital elevation model (DEM) into a relative elevation model normalized to the stream network (Figure 6, adapted from Rebolho et al., 2018). The process starts with a DEM, which provides the raw terrain elevations for the catchment. From this, a drainage direction grid

is computed, assigning each cell its steepest descent path, defining how surface water will flow across the landscape. By accumulating flow from upstream cells, drainage areas are calculated; high accumulation values indicate channel cells.

The HAND value for each cell is then determined as the difference between its elevation and the elevation of the nearest channel thalweg cell along its drainage path. This represents the additional water depth required for inundation in that cell. The resulting HAND raster forms a relative elevation model (REM) that captures the vertical distance from land surface to the river network, providing the foundation for scenario-based flood inundation mapping. All layers are precomputed by OWP-FIM (NOAA Office of Water Prediction, 2025) and organized as rasters at the HUC-8 level for efficient retrieval and application within the platform.

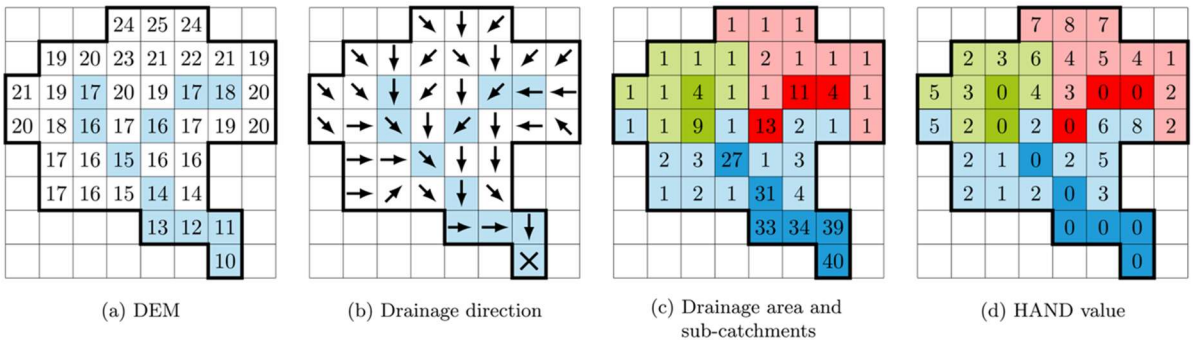

Figure 6. Schematic of HAND model calculation for FIM generation. Adapted from Rebolho et al. (2018).

Each LP is further subdivided into HydroID-defined, reach-scale catchments. A HydroID is the unique identifier assigned in the OWP Hydrofabric to a modeling reach and its associated catchment. Because NHDPlus reaches can be split into multiple modeling units, a single COMID may correspond to several HydroIDs. Each HydroID catchment represents the drainage area contributing to its reach outlet and is the unit to which HAND elevations and hydraulic properties are applied (Figure S1 in supplementary material). Reach-specific parameters, including average channel geometry, Manning's roughness, and local slope, are linked to each HydroID.

Stage values must be provided to generate flood inundation maps using the HAND model. To generate inundation extents from discharge-based inputs, discharge values are converted to stage values, which are then used as HAND model inputs. Synthetic rating curves (SRCs) are extracted from the OWP-FIM framework (Figure 7). These SRCs are derived using Manning's equation applied to reach-averaged channel properties and provide the discharge-stage relationships used for each HydroID catchment. Once retrieved, SRCs are cached locally (in IndexedDB) to enable efficient, real-time performance during interactive scenario modeling.

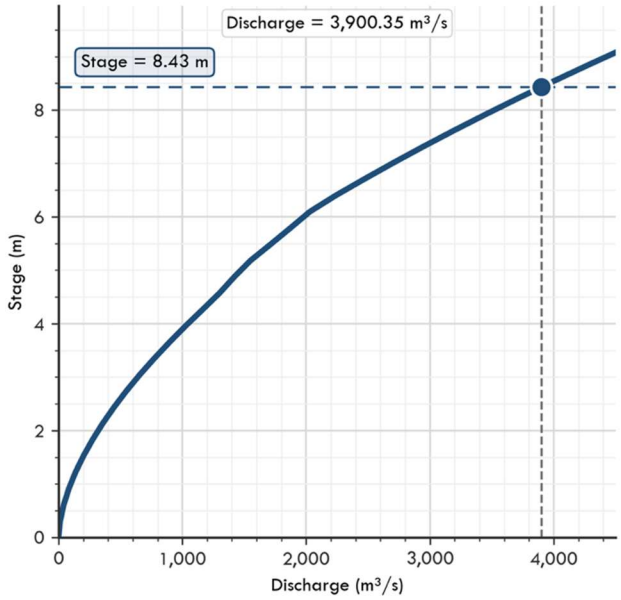

Figure 7. Synthetic stage-discharge rating curves for the Bellevue, Nebraska, river reach (COMID: 940230064) with OWP-FIM v.4.5.2.11.

3.2. Real-Time Flood Inundation Mapping

The system provides two complementary modes for scenario development. In "master discharge" mode, a discharge value is specified once for the selected reach, and the corresponding stages for all HydroID catchments are obtained by applying their respective synthetic rating curves (SRCs). This ensures a consistent, reach-wide baseline and allows users to inspect stage values per catchment without additional input. In "individual control" mode, users can override the baseline and assign stage values individually to each HydroID catchment using interactive sliders. This functionality supports the exploration of hydrological variability along the reach, where differences in local slope, channel geometry, or Manning's roughness generate distinct inundation patterns. Both modes feature bidirectional conversion between discharge and stage via linear interpolation on the SRCs.

Integration with the National Water Model extends these capabilities by automatically converting forecast discharges into catchment-specific stages. Users can generate scenarios from retrospective NWM 3.0 data (1980-2022) (Cosgrove et al., 2024) or from forecasts with horizons of 24 hours, 10 days, and 30 days. The platform generates flood maps entirely in the browser through client-side geospatial processing. The system uses the Geospatial Data Abstraction Library (GDAL), which is compiled to WebAssembly (WASM) via the Loam library (Dohler, 2022), to enable web-native geospatial operations without server dependencies.

This architecture allows reprojection between EPSG:5070 (NAD83 Conus Albers) and EPSG:4326 (WGS84), with raster datasets stored on the client side at the HUC-8 level. In addition, the Loam library crops raster datasets on the fly to include only the areas relevant to the current scenario, significantly reducing processing resources compared to processing entire HUC-8 datasets. The system maintains HUC-8-specific IndexedDB databases for caching relative

elevation models, rating curves, and catchment reference raster datasets, thereby eliminating redundant data transfers across repeated analysis sessions.

The architecture also employs Web Workers to enable concurrent processing and maintain a responsive user interface during computationally intensive operations. Raster cropping, raster mosaicking, stage-discharge conversions, and flood depth calculations execute in background threads, allowing users to continue interacting with the interface while scenarios are generated. Progress indicators provide real-time feedback on processing status. Runtime depends on the selected analysis extent, raster volume, and the number of structures considered in subsequent impact analysis; representative browser-side benchmark results across nested spatial extents are reported in Section 4.4. The system processes flood calculations in discrete batches to manage memory usage during extended analysis sessions.

Internally, the workflow applies the specified stage to the REM for each HydroID catchment. Flood depth at each pixel is computed as stage minus REM, and the raster datasets are then mosaicked to form the inundation map. Depths are displayed on the map using a blue gradient that varies by severity. The complete computational workflow integrating web worker spawning, raster processing, flood mapping, and damage calculation is presented in Figure 8. This pseudocode illustrates the systematic approach, from initial data preparation to final infrastructure impact assessment, highlighting the platform's client-side processing capabilities and optimization strategies.

3.3. Infrastructure Impact Assessment

Building upon the flood inundation mapping capabilities discussed in Section 3.2, the platform extends scenario analysis to include comprehensive infrastructure impact assessment and economic damage estimation. This process converts raw flood depth predictions into actionable decision support by quantifying potential impacts on local infrastructure. The infrastructure impact assessment uses the National Structure Inventory (U.S. Army Corps of Engineers, 2022) to identify and characterize buildings in flood-prone areas. NSI provides comprehensive building-level data, including occupancy classifications, structural characteristics, economic valuations, and population estimates for structures across the United States. Structure discovery uses the optimal bounds calculated during flood scenario generation, requesting data only within the precise extent determined by its HydroID catchments. To optimize performance during iterative scenario development, a caching strategy is employed. Upon initial selection of a river reach, all structures within the calculated optimal bounds area are downloaded and locally cached. Subsequent damage calculations occur instantly as users adjust flood scenarios, enabling real-time updates on impact assessment.

Economic impacts are quantified using damage functions from the FEMA Hazus methodology (Alabbad et al., 2023; Scawthorn et al., 2006; Sufi et al., 2025), which provides a standardized framework for estimating flood damage. Hazus provides empirically derived damage functions that relate flood depth to expected damage percentages for various building types, based on extensive field data and engineering analysis. These depth-damage relationships form the foundation for assessing economic impacts across diverse occupancy classifications. This

implementation includes a spectrum of occupancy types, including residential (RES1-RES6), commercial (COM1-COM10), industrial (IND1-IND6), and specialized categories for agricultural, educational, government, and religious facilities. Each occupancy type has distinct vulnerability characteristics, represented in Hazus by occupancy-specific damage curves for structures and contents. Occupancy classification mapping accommodates NSI's detailed building codes by assigning them to corresponding base Hazus categories. Multi-variant residential codes, such as "RES1-2SWB" from NSI, are mapped to base "RES1" curves, while detailed commercial subcategories use the most appropriate COM category. Linear interpolation between Hazus curve points enables the precise calculation of damage percentages for any flood depth.

Algorithm 1: Client-Side Flood Map Generation with Multi-Branch Processing

Require: Selected time t, watershed HUC8
modeled reaches $C = \{\text{COMID}\}$
Ensure: Georeferenced flood depth raster M_{geo}

Phase 1: Data Retrieval
$DB \leftarrow \text{IndexedDB.open}(HUC8)$
$K \leftarrow \text{getCatchmentsForReaches}(C)$
$Q_c \leftarrow \text{extractStreamflow}(C, t)$
$RC \leftarrow \text{getStageDischargeCurves}(K)$

Phase 2: Discharge to Stage
for branch $b \in Branches(K)$, **do**
  catchment $k \in b$
  $S_k \leftarrow \text{interpolate}(Q_{c(k)}, RC(k))$
end for

Phase 3: Optimal Bounds
$B_{optimal} \leftarrow \bigcup_{k:S_k>0} DB.bounds(k)$
$B_{buffered} \leftarrow B_{optimal}$ +500m buffer

Phase 4: Native Raster Windowing
for branch $b \in Branches(K)$ **do**
  $R_{elev}(b), R_{catch}(b) \leftarrow DB[b]$
  $T_{elev}(b) \leftarrow \text{cropWindow}(R_{elev}(b), B_{buffered})$
  $T_{catch}(b) \leftarrow \text{cropWindow}(R_{catch}(b), B_{buffered})$
end for

Phase 5: Flood Depth Calculation
for branch $b \in Branches(K)$ **do**
  $R_{flood}(b) \leftarrow \text{Float32Array}(W \times H).fill(0)$
  for pixel i in raster **do**
    $k_{id} \leftarrow T_{catch}(b)[i]$
    $d \leftarrow S_{k_{id}} - T_{elev}(b)[i]$
    if $d > d_{min}$ **then**
      $R_{flood}(b)[i] \leftarrow d$
    end if
  end for
end for

Phase 6: Max-Depth Mosaicking
$M_{geo} \leftarrow \text{createGeoRaster}(\text{pixelwiseMax}(\{R_{flood}(b)\}), B_{buffered})$

return M_{geo}

Figure 8. Pseudocode for generating the flood inundation raster.

Flood depth integration with Hazus damage curves enables the instantaneous calculation of economic impact for each structure within affected areas (Mostafiz et al., 2021). The computational workflow extracts site-specific flood depths at building footprints, applies appropriate depth-damage functions, and converts damage percentages to monetary losses using NSI-reported structure and contents valuations. Structural damage refers to physical impacts on a building's framework, foundation, and integrated systems, whereas content damage includes

impacts on movable property, including furnishings, equipment, and inventory. Damage severity is visualized using a standardized color scale: light amber (<25%), orange (25-50%), red (50-75%), and purple (>75%). Interactive building-level tooltips display sampled flood depth, assigned occupancy code, structure and contents damage percentages, and corresponding monetary losses. Summary statistics report the number of affected buildings, aggregate structural losses, and aggregate contents losses. A typical interface display combining flood inundation output with affected-structure and damage information is shown in Figure 9. The interface presents inundation extent, affected buildings, and summary loss statistics in a single scenario analysis view.

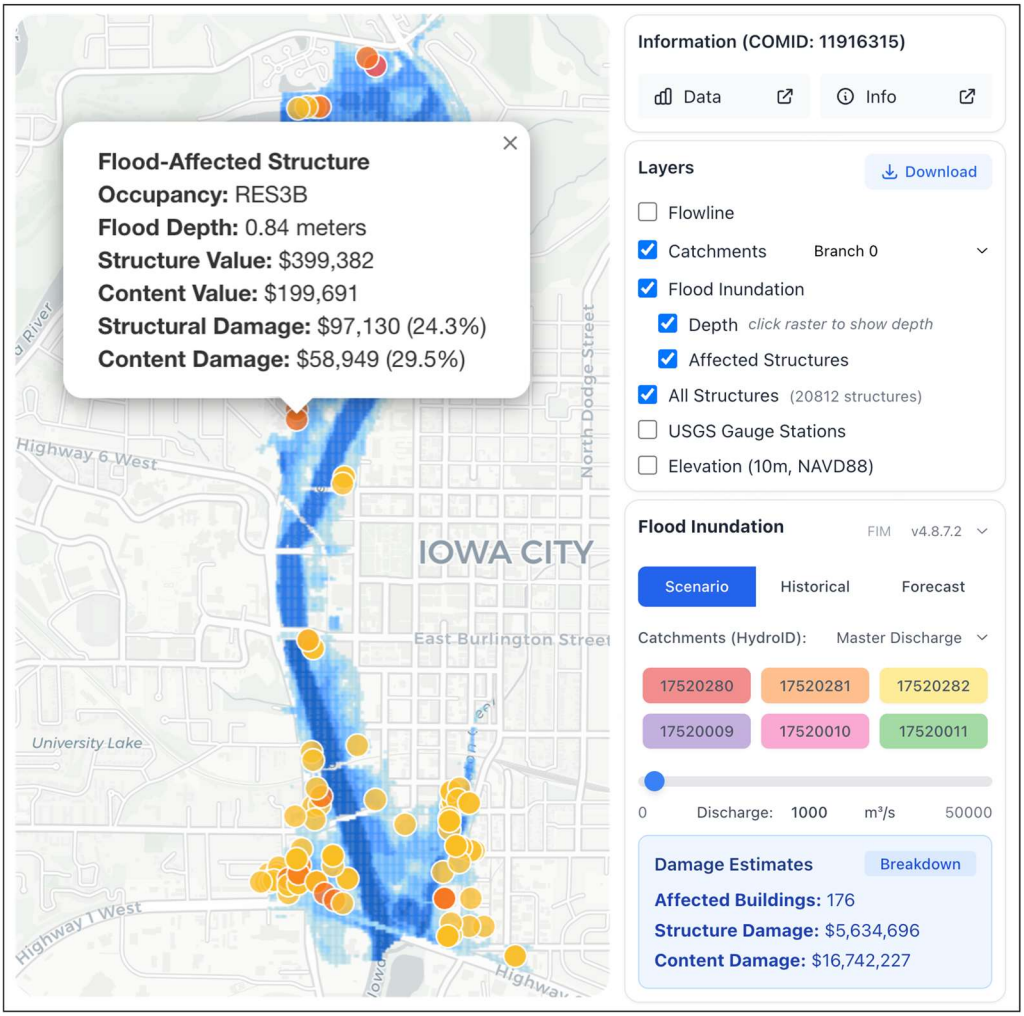

Figure 9. Flood inundation mapping user interface display with flood inundation and affected structures layers. Users can generate inundation extents through scenario-based modeling using a discharge input or National Water Model historical and forecast values.

4. Results and Discussion

We highlight the application's generalizability, scalability, and applicability through a case study across two affected areas during the 2019 Midwestern flooding events. This case study

demonstrates the platform's capabilities in real-world disaster scenarios, enabling comparisons against observed flood extents and other inundation mapping platforms.

4.1. Case Study: The 2019 Midwestern Floods

The 2019 Midwestern floods were among the most significant and widespread flood events in recent U.S. history, affecting multiple states across the Missouri and Mississippi River basins from March through September. The flooding was triggered by an exceptionally wet spring season, characterized by record-breaking precipitation totals and rapid snowmelt, which saturated soils and led to excessive runoff throughout the region (Velásquez et al., 2023). The event resulted in extensive agricultural losses and infrastructure damage and required numerous flood emergency responses across Iowa, Nebraska, Missouri, and surrounding states (Kraft et al., 2023).

This case study examines two representative areas that experienced severe flooding: Des Moines, Iowa, and Bellevue, Nebraska. Two representative HUC-12 watersheds (071000061703 in Des Moines, IA; 102300060603 in Bellevue, NE) were selected to demonstrate the platform's ability to generate flood scenarios. The case study was performed on an M4 MacBook Air with Chrome version 140, Firefox version 142, and Safari version 18.5. All core functionalities performed as expected across the tested browsers. Minor rendering artifacts were observed in Safari, but they did not impair analytical capabilities. This may be attributable to limited support for newer browser features in Safari (Sabaren et al., 2018).

The Des Moines area demonstrated the platform's flood-mapping capabilities during the 2019 Midwestern floods. The platform successfully captured the spatial patterns of flooding observed in satellite imagery (NASA Science, 2019b), demonstrating its ability to translate National Water Model discharge predictions into realistic flood-extent visualizations using the OWP-FIM methodology. Additionally, the platform's outputs were compared with Iowa Flood Center mapping products for the same flood event available on the Iowa Flood Information System (IFIS). These maps were developed using physics-based hydrodynamic models and validated by the Iowa Flood Center with field observations and high-resolution terrain data (Demir & Krajewski, 2013).

These IFIS maps represent flood conditions in select Iowa communities at half-foot stage intervals. The closest flood map to this study corresponds to a discharge of 776 m^3/s. In comparison, the platform-generated maps use 813 m^3/s from NWM retrospective data, ensuring similar conditions. Figure 10 displays the comparisons among these maps. These comparisons reveal strong spatial agreement between platform outputs and IFIS products, as well as observed extents. The platform successfully captures flooding patterns along the Raccoon River corridor, including inundation of floodplain areas, recreational zones, and low-lying development areas that experienced flooding during the 2019 event.

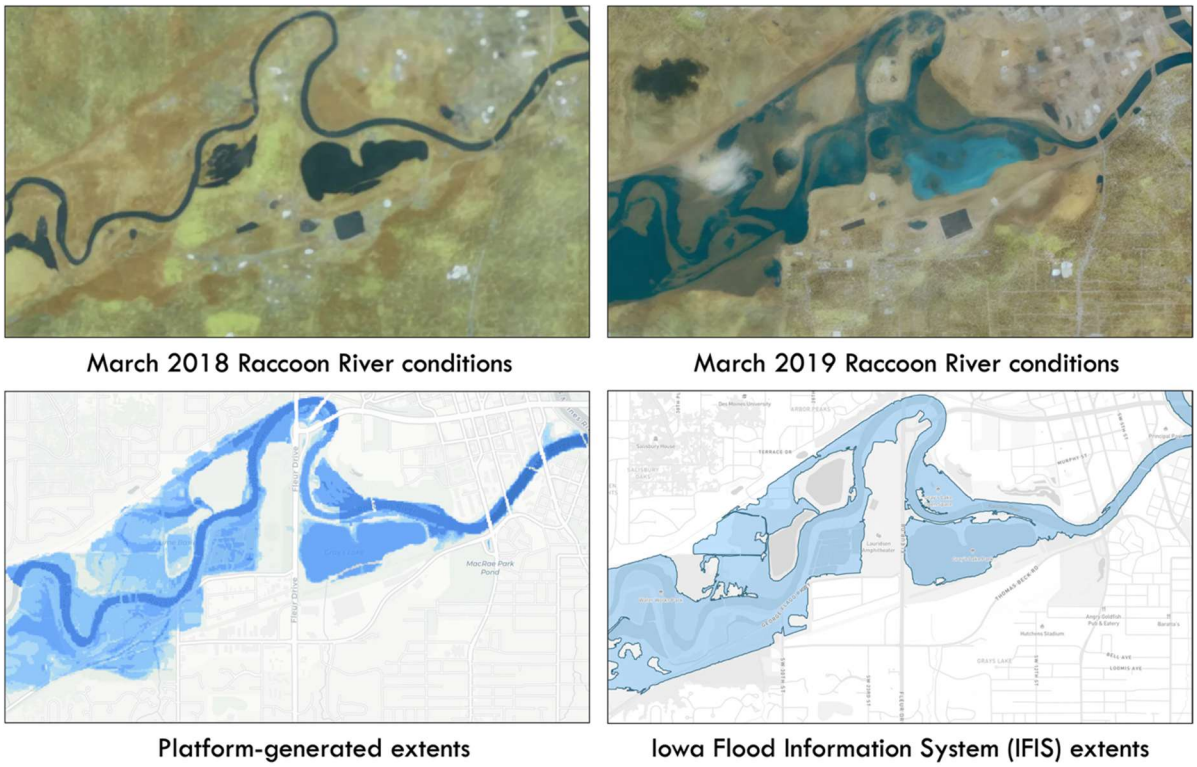

Figure 10. Comparison of pre-flood and flood conditions (NASA Science, 2019b) in the Raccoon River corridor near Des Moines, Iowa, alongside model outputs from the platform and the Iowa Flood Information System (IFIS). (Top left) Satellite imagery for March 15, 2018, under standard conditions; (Top right) Satellite imagery following the floods on March 18, 2019; (Bottom left) Flood inundation map generated by the platform (OWP-FIM v.4.5.2.11) for a discharge of 813 **m³/s**, corresponding to NWM retrospective conditions; (Bottom right) Corresponding Iowa Flood Information System (IFIS) flood inundation map for the closest available discharge condition, 776 **m³/s** (Demir & Krajewski, 2013).

4.2. Flood Extent Evaluation and HAND Methodology Assessment

Bellevue, Nebraska, was selected as the region of interest for evaluating the generated flood extents. This case study provides an opportunity to evaluate the accuracy of the platform's flood extent predictions, assess the performance of the underlying HAND methodology in representing real-world flood conditions, and test the functionality for assessing infrastructure damage. Before conducting a quantitative comparison, the platform's time-series visualization capabilities were utilized to examine historical discharge during the March 2019 event. Due to limited data availability at stations directly within the Bellevue study area, where monitoring stations were either newly established or lacked complete 2019 flood records, time-series analysis was conducted using the USGS gauge station near Omaha, Nebraska (USGS-06610000).

This case study revealed significant discharge magnitudes during the peak flooding period, with USGS observed data showing flows of 4,729 m³/s, while National Water Model retrospective data estimated approximately 3,900 m³/s for March 16, 2019, at 17:00 UTC (Figure 11). Although

such model-observation discrepancies are well documented in hydrologic forecasting, the platform remains flexible by accommodating different discharge sources by accepting user-supplied discharge inputs (e.g., local gauge records, USGS observations, or synthetic hydrographs) to generate inundation extents.

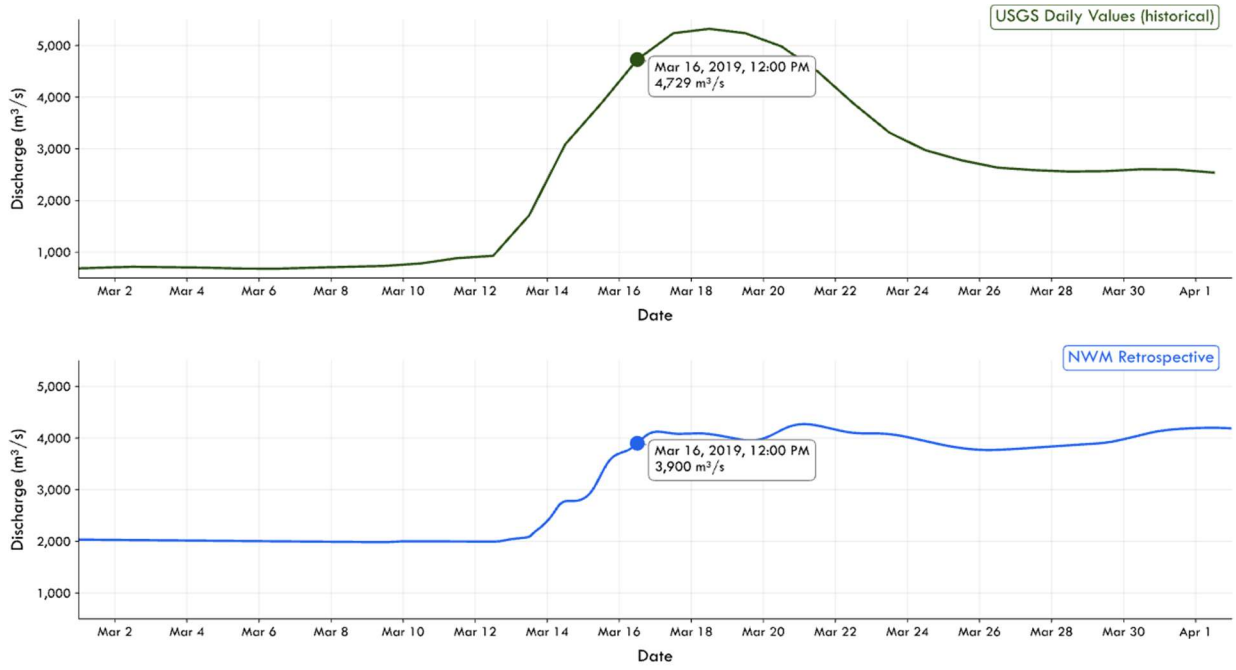

Figure 11. Time-series discharge data for the Bellevue, Nebraska, case study area on March 16, 2019, at 12:00 p.m. CDT. (Top) USGS gauge observations from station 06610000 near Omaha, Nebraska. (Bottom) NWM retrospective discharge for the corresponding Missouri River reach in Bellevue, Nebraska (COMID: 940230064).

A quantitative assessment of platform-generated flood maps was conducted through a confusion matrix (Townsend, 1971), comparing platform outputs against observed flood conditions during the March 2019 event. We used the Landsat Collection 2 Level 3 Dynamic Surface Water Extent (DSWE) Science Products, obtained from the Earth Resources Observation and Science (EROS) Center (2022), as the reference dataset for a binary flood-inundation raster. For the case study in Bellevue, Nebraska, the platform-generated inundation map was produced using OWP-FIM v.4.5.2.11, as this version more closely matched the observed flood extents than v.4.8.7.2. Figure 12 illustrates the comparison between 2018 pre-flood conditions, observed 2019 flooding (NASA Science, 2019a), and the platform-generated flood maps.

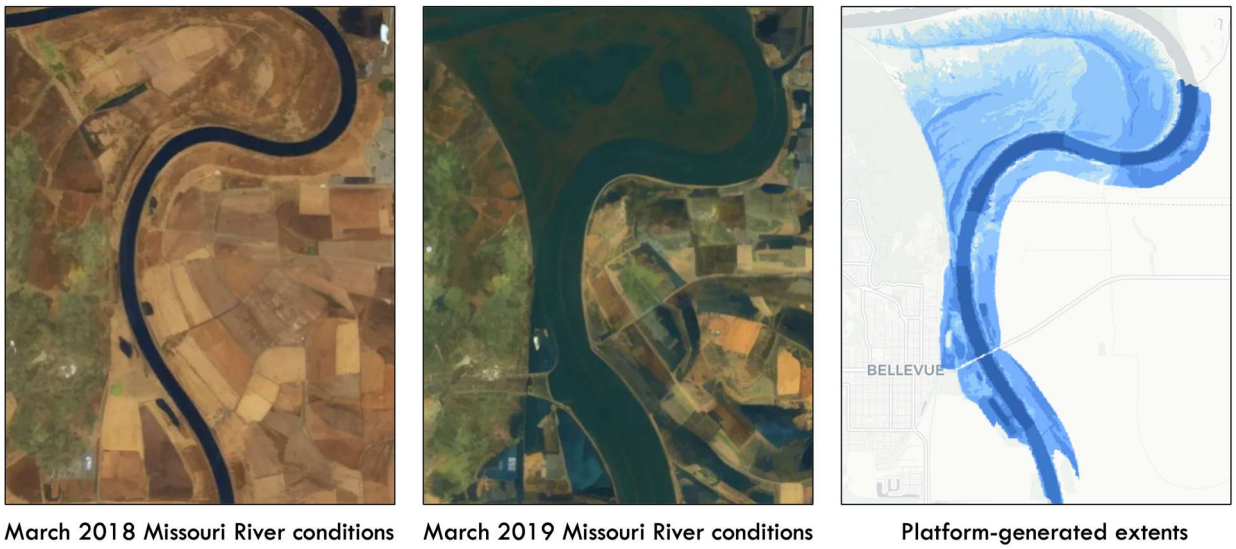

Figure 12. Comparison of pre-flood and flood conditions (NASA Science, 2019a) for the Missouri River reach near Bellevue, Nebraska, alongside model output from the platform. (Left) Satellite imagery for March 20, 2018, under standard conditions; (Middle) Satellite imagery following the floods on March 16, 2019; (Right) Flood inundation map generated by the platform (OWP-FIM v.4.5.2.11) for a discharge of 3,900 m^3/s, corresponding to NWM retrospective conditions.

The validation process involved pixel-level alignment between the platform output and the Landsat Collection 2 Level-3 Dynamic Surface Water Extent (DSWE) reference raster. Both datasets were reprojected to EPSG:5070, after which pixelwise comparisons were performed. For the Landsat DSWE interpreted layer, pixel values 1, 2, and 3, corresponding to high-confidence water, moderate-confidence water, and potential wetland, respectively, were recoded as inundated to generate the binary observed flood-extent map used in the validation. The observed, platform-generated, and binary extent maps are shown in Figure 13.

Using these aligned binary rasters, a confusion matrix was then used to quantify agreement between platform predictions and observed flood conditions across seven distinct HydroID catchment regions within the study area (Figure 14). Platform performance was quantified using Percent Correct, Recall, Precision, F1, and IoU metrics to compare generated flood extents against observed conditions. These metrics offer complementary perspectives on flood-mapping accuracy by assessing different aspects of predictive performance.]

True positives (TP) represent pixels correctly identified as flooded by both the platform and reference data. False positives (FP) are pixels incorrectly predicted as flooded by the platform but not flooded in the reference data. True negatives (TN) represent pixels correctly identified as non-flooded by both datasets, while false negatives (FN) are pixels that were flooded but missed by the platform predictions. Percent Correct measures overall accuracy by calculating the proportion of correctly identified pixels relative to the total number of pixels analyzed (Eq. 1).

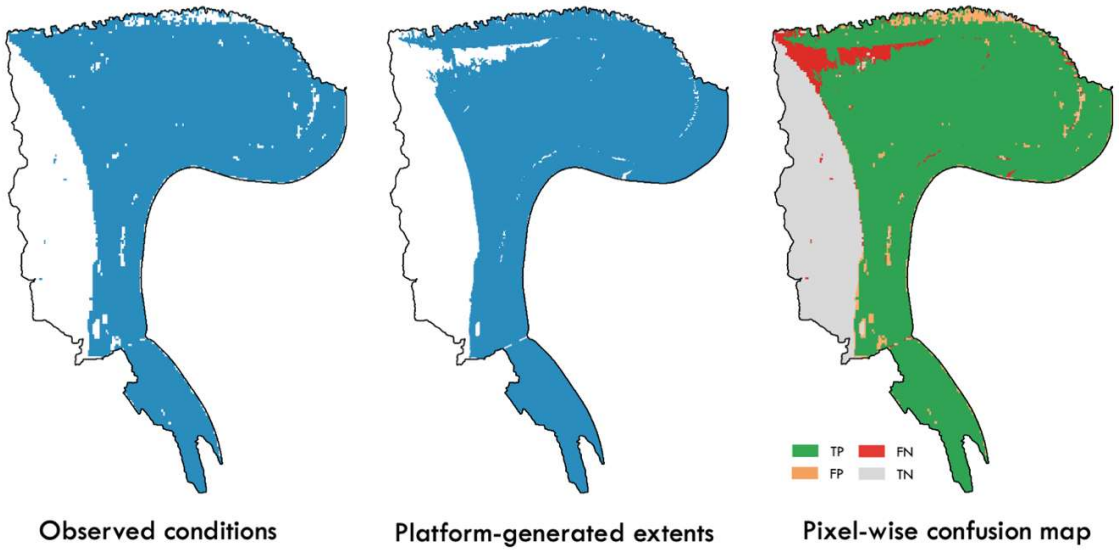

Figure 13. (Left) Observed flood extent derived from the Landsat Collection 2 Level 3 Dynamic Surface Water Extent product; (Middle) platform-generated inundation extents; (Right) Pixel-wise confusion map displaying the spatial distribution of true positives (TP), false positives (FP), false negatives (FN), and true negatives (TN).

$$\text{Percent Correct} = \frac{TP + TN}{TP + FP + FN + TN} \quad \text{(Eq. 1)}$$

Recall, also known as sensitivity or hit rate, represents the platform's ability to detect flooded areas correctly (Eq. 2):

$$\text{Recall} = \frac{TP}{TP + FN} \quad \text{(Eq. 2)}$$

Precision quantifies the reliability of flood predictions by measuring the proportion of predicted flooded pixels that were actually flooded (Eq. 3):

$$\text{Precision} = \frac{TP}{TP + FP} \quad \text{(Eq. 3)}$$

The F1 score provides a balanced summary of flood mapping performance by combining Recall and Precision into a single metric. It is particularly useful when both omission errors (FN) and commission errors (FP) are important. The F1 score is defined as the harmonic mean of Precision and Recall (Eq. 4):

$$F1 = \frac{2TP}{2TP + FP + FN} \quad \text{(Eq. 4)}$$

Intersection over Union (IoU) (Eq. 5), also known as the Jaccard Index, measures the spatial overlap between the predicted and reference flooded areas relative to their combined extent. This metric provides a stricter assessment of agreement because it penalizes both overprediction and underprediction:

$$IoU = \frac{TP}{TP + FP + FN} \quad \text{(Eq. 5)}$$

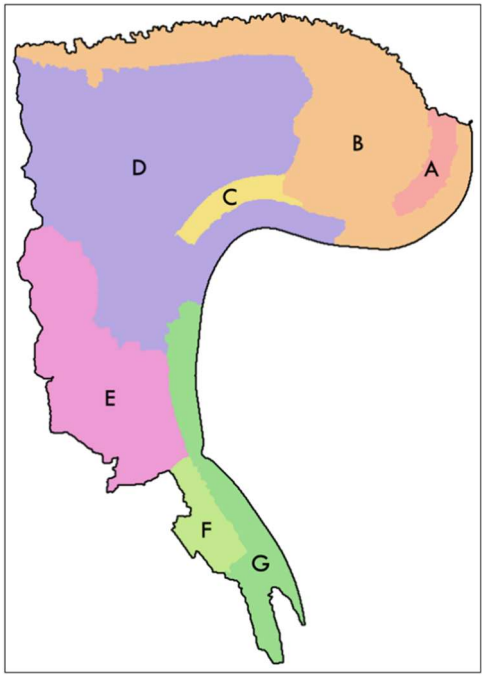

Figure 14. Seven HydroID catchments used in the flood extent assessment for the Bellevue, Nebraska, case study, labeled as areas A through G.

The validation results indicate strong overall agreement between platform-generated and observed flood extents across the seven assessment areas (Table 1). Area C exhibited perfect agreement across all reported metrics, while Areas A, B, F, and G also showed strong performance. Performance was comparatively lower in Areas D and E, although for different reasons. In Area D, Precision remained very high (0.9899) while Recall was lower (0.9010), indicating that false negatives contributed more to the reduced scores than false positives. This is evident in the high concentration of false negative pixels in Area D (Figure 13). In Area E, Recall remained high (0.9949), but Precision (0.8805) and IoU (0.8766) were comparatively lower, indicating a greater influence of false positives and reduced spatial overlap. Overall, these results suggest that the

platform reproduced observed flood extent patterns well across most of the study area, with localized variability in omission and commission errors across catchment areas. Taken together, the results support the use of the platform for exploratory analysis, rapid situational awareness, and preliminary decision support across the continental United States.

Table 1. Performance metrics for the seven validation regions (A-G) comparing platform inundation extents to observed flood extents for the March 16, 2019 (17:00 UTC) flood in Bellevue, NE.

Area	PC	Recall	Precision	F1	IoU
A	0.9535	1.0000	0.9535	0.9762	0.9535
B	0.9116	0.9708	0.9359	0.9530	0.9103
C	1.0000	1.0000	1.0000	1.0000	1.0000
D	0.9187	0.9010	0.9899	0.9433	0.8928
E	0.9662	0.9949	0.8805	0.9342	0.8766
F	0.9821	0.9956	0.9862	0.9909	0.9820
G	0.9554	0.9913	0.9628	0.9768	0.9547

To further assess consistency with the original OWP-FIM implementation, platform-generated inundation extents were compared with official FIMServ outputs for OWP-FIM versions 4.5.2.11 and 4.8.7.2. FIMServ is a Python service for official OWP-FIM inundation products (Baruah et al., 2025a). Because the platform uses the same OWP-FIM methodology and underlying input datasets, this comparison should be interpreted as an assessment of implementation fidelity. For the March 16, 2019, Bellevue event (17:00 UTC), the platform reproduced the corresponding FIMServ inundation extents, resulting in identical agreement metrics when both products were evaluated against the observed benchmark. These results indicate that the web platform preserves the behavior of the original OWP-FIM model while extending it through a web-based interface and additional analytical functionality. Table 2 presents the whole-catchment comparison of the platform and FIMServ against the observed flood extents.

Table 2. Flood extent validation results for March 16, 2019 (17:00 UTC) in Bellevue, NE, comparing platform outputs and FIMServ (Baruah et al., 2025a) OWP HAND-FIM outputs against the observed inundation extents. OWP-FIM versions v.4.5.2.11 and v.4.8.7.2 were tested.

Comparison (vs observed)	PC	Recall	Precision	F1	IoU
Platform (v.4.5.2.11)	0.9328	0.9483	0.9605	0.9544	0.9128

FIMServ (v.4.5.2.11)	0.9328	0.9483	0.9605	0.9544	0.9128
Platform (v.4.8.7.2)	0.6325	0.5067	0.9953	0.6716	0.5055
FIMServ (v.4.8.7.2)	0.6325	0.5067	0.9953	0.6716	0.5055

4.3. Evaluation of Impacted Infrastructure

Focusing on the heavily affected Bellevue region, the platform's infrastructure impact assessment capabilities were evaluated by intersecting flood extent outputs with building footprints and occupancy information from the National Structure Inventory (NSI). The platform identified 22 flood-affected structures within the Bellevue study area. For each affected structure, the system estimated structural and content losses using Hazus depth-damage relationships based on the representative flood depth extracted at the structure location. The affected structures and damage classifications produced by the platform are shown in Figure 15.

These results demonstrate the practical value of linking rapid flood mapping with structure-level damage estimation in a browser-based environment. The resulting loss estimates are most appropriate for screening-level interpretation because of challenges with the HAND approach for flood inundation mapping and the assumptions embedded in the Hazus framework.

4.4. Performance Evaluation and Limitations

The client-side architecture enabled browser-based flood inundation mapping on modern consumer hardware. Representative end-user runtimes for the main workflow stages are summarized in Table 3. To evaluate browser-side computational scaling across a broader range of regional settings, we benchmarked nested HUC-12, HUC-10, and HUC-8 analyses in eight contrasting CONUS watersheds centered on Boston, Massachusetts; Raleigh, North Carolina; Houston, Texas; Iowa City, Iowa; Bellevue, Nebraska; Albuquerque, New Mexico; Riverside, California; and Portland, Oregon. This was done to account for landscape variability and different HUC sizes. The resulting browser-side runtime scaling with number of pixels processed is shown in Figure 16. Benchmarks were recorded on an M4 MacBook Air using Chrome version 140.

Each HUC-8 FIM dataset was prepared separately as a one-time local step and is not included in the browser-side benchmark times reported here. For each benchmark case, the runtime was recorded three times under identical hardware and browser settings, and Figure 16 shows the average runtime. Processed pixels were measured from the cropped native-resolution raster windows used by the browser-side analysis pipeline before display downsampling, making this metric a direct measure of raster workload.

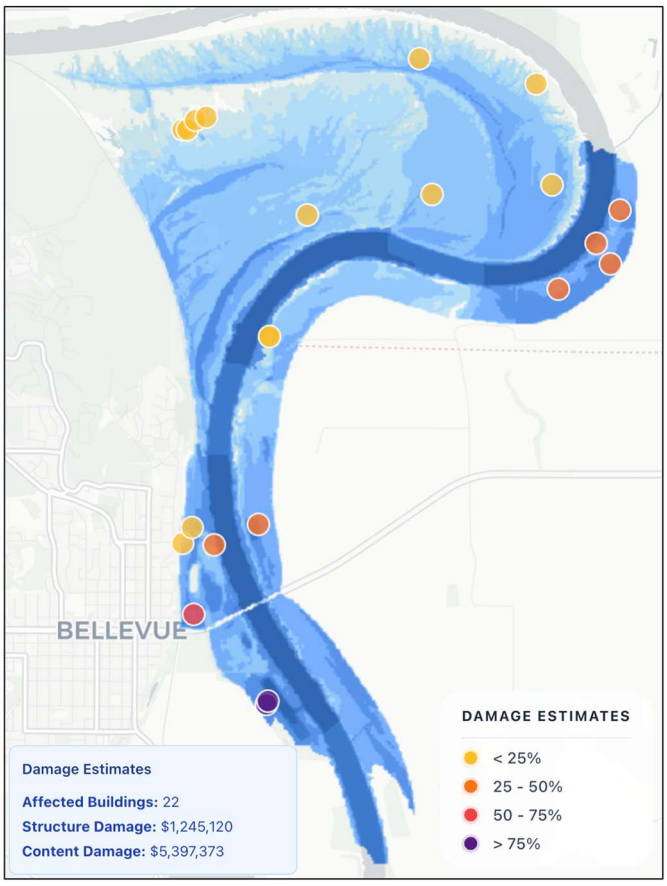

Figure 15. Damage assessment results for Bellevue, Nebraska. Points represent flood-affected structures, colored by damage severity: light amber (<25%), orange (25-50%), red (50-75%), and purple (>75%).

Table 3. Representative performance benchmarks on a modern desktop browser at the river reach level (*Tested on Wi-Fi at 100 Mbps speeds. **Tested on an M4 MacBook Air, Chrome version 140)

Task	Runtime	Interpretation
Initial FIM download	47 s	One-time setup
Initial scenario	4-8 s	On-demand analysis
Damage assessment	1-2 s	Impact screening
Scenario re-render	< 0.6 s	Real-time interaction

The browser-side runtime progressively increased with the number of pixels processed across the 24 benchmark cases evaluated in this study (Figure 16). The average runtime by scale increased from 2.76 seconds for HUC-12 analyses to 7.17 seconds for HUC-10 analyses and 15.06 seconds for HUC-8 analyses. The clear link between processed pixels and browser-side performance suggests that performance is more closely associated with the cropped raster workload rather than with the watershed size alone. However, deviations from the overall trend indicate that pixel count

does not solely determine runtime. For example, cases like Buffalo-San Jacinto HUC-8 and Lower Willamette HUC-8, which fall below the trend, imply that additional factors such as watershed-specific network complexity also play a role. Some shorter HUC-12 cases also exhibited more variability between runs, indicating that the overhead from browser or service warm-up has a larger proportional impact on shorter analyses than on longer HUC-8 runs.

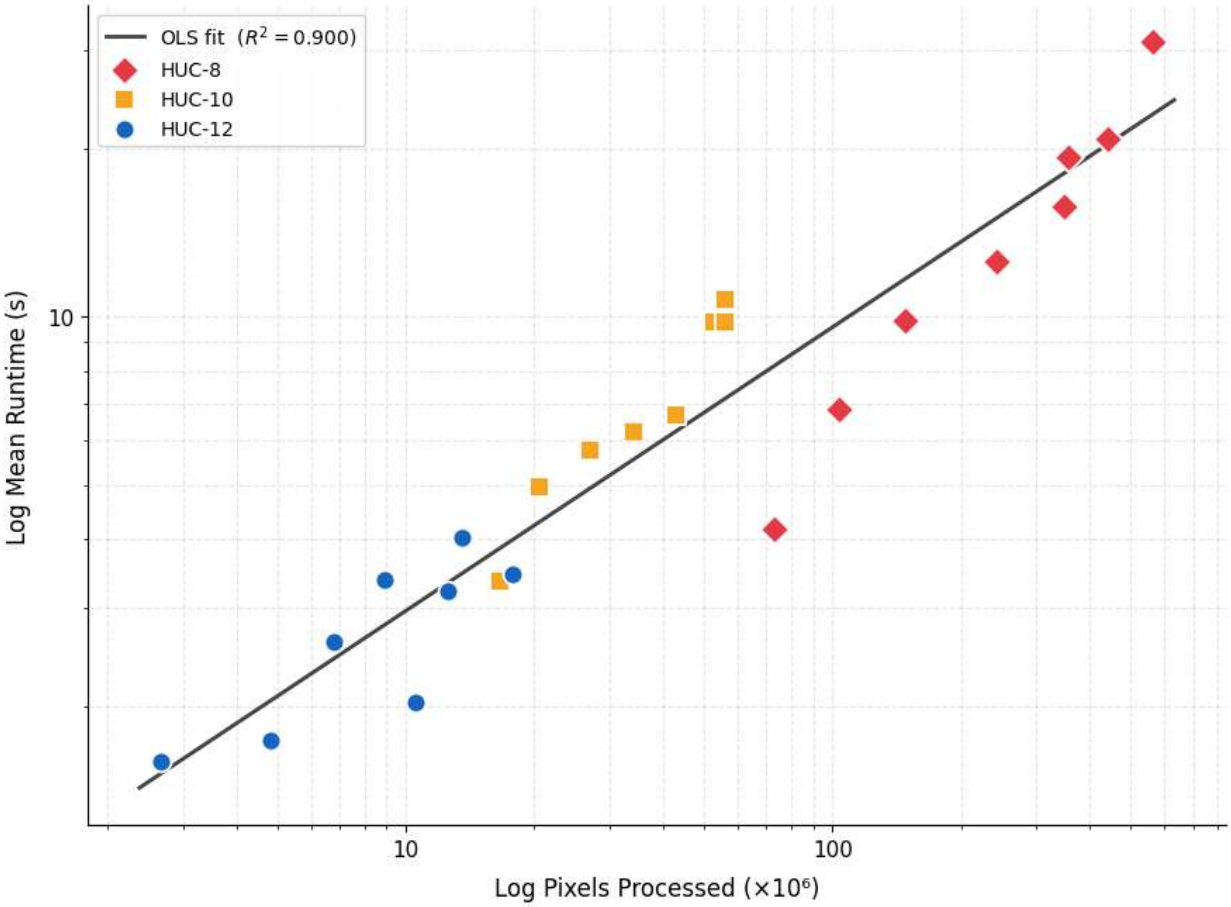

Figure 16. Browser-side runtime versus processed pixels across HUC-12, HUC-10, and HUC-8 benchmark cases. The number of pixels represent the cropped native-resolution raster cells included in the analysis before display downsampling. Each point indicates the average of three runs. The figure is in log-log scale.

The platform's predictive accuracy is fundamentally tied to the assumptions and limitations of the underlying flood-mapping and damage-estimation datasets (Tomkins, 2012). Although the HAND-based framework provides a computationally efficient approach for rapid regional inundation assessment, it does not explicitly resolve complex hydraulic processes such as backwater effects, flow obstruction by transportation or urban infrastructure, levee influences, or levee breach dynamics (Costabile et al., 2026; Dazzi et al., 2019; Xing et al., 2025). In addition, the multi-pass depth surfaces used in the OWP HAND-FIM workflow may contain localized patchiness or raster artifacts, which can affect the consistency of modeled water depth at the structure scale. These limitations become especially important when modeled inundation depths

are propagated to structure-level damage estimates, since errors in local flood depth and extent directly influence the resulting loss calculations. Prior work has shown that detailed building-level flood exposure analysis and urban flood assessment can be sensitive to hydraulic representation, spatial resolution, and local flow complexity, particularly in developed environments and hydraulically controlled settings (Bertsch et al., 2022; Xing et al., 2025). Accordingly, the platform's water-depth outputs should be interpreted primarily as screening-level indicators of inundation severity rather than precise local hydraulic predictions. Additional benchmarking of modeled water depth against independent local observations or reference products would further improve understanding of uncertainty in the depth and damage outputs.

The damage estimates are also conditioned on the assumptions of the FEMA Hazus depth-damage framework. Hazus provides a practical, standardized basis for rapid estimation at scale, but it simplifies damage assessment by relying primarily on inundation depth and generalized occupancy classes. As noted in the literature, damage severity also depends on additional hydraulic characteristics, including flow velocity and related impact processes, which are not explicitly represented in a depth-only formulation (Lazzarin et al., 2022; Wang, 2025). Furthermore, the monetary losses reported by the platform should be interpreted as first-order, screening-level estimates instead of parcel-specific or engineering-grade damage determinations. This interpretation is especially important in locations where localized depth artifacts or unresolved hydraulic controls may influence structure-level depth assignment.

5. Conclusions

This study presents a comprehensive generalized client-side platform for flood inundation mapping and infrastructure impact assessment. By integrating federal datasets from OWP-FIM and NWM within a browser-based architecture, we overcome the accessibility and cost barriers of traditional desktop and server-dependent systems. The 2019 Midwestern floods case study demonstrated the platform's ability to produce flood extents and screening-level damage estimates that compared favorably with observed data and official products, supporting its use in real-world rapid assessment settings.

The platform's performance, analytical scope, and decision-support capabilities can be further enhanced in future studies. For performance, adopting WebGPU could harness client-side graphics processing units to parallelize raster operations, thereby reducing computation time and enabling the analysis of larger geographic extents. The platform's analytical capabilities could be further enhanced by incorporating additional impact models, such as those for quantifying agricultural losses or modeling disruptions to transportation networks. To better support planning and mitigation efforts, interactive tools will be developed that allow users to simulate interventions, such as proposed levees, and receive immediate visual feedback on how such changes affect flood extents. Finally, to support analyses that exceed the practical limits of client-side processing, a hybrid architecture will be investigated to provide a scalable solution that accommodates both rapid, localized assessments and more extensive, regional-scale studies.

This work demonstrates that web-based flood modeling can serve as a viable complement to traditional approaches, showing that browser-based platforms can support rapid flood extent analysis and preliminary consequence assessment for planning, communication, and emergency management. The platform bridges the gap between sophisticated scientific tools and practical decision-support applications, enabling broader stakeholder participation in flood risk assessment and emergency planning. As web technologies advance and federal datasets become more accessible, platforms of this type will provide critical tools that support the democratization of hydrological modeling and improve water resources decision-making.

6. Declaration of AI-Assisted Technologies

During the preparation of this work, the authors used ChatGPT to improve the flow of the text, correct any potential grammatical errors, and improve the writing. After using this tool, the authors reviewed and edited the content as needed and took full responsibility for the content of the publication.

7. References

Agafonkin, V. (2020). Geobuf: A compact binary encoding for geographic data. (v.3.0.2) [Software Library]. https://github.com/mapbox/geobuf

Agafonkin, V. (2023). Leaflet: JavaScript library for mobile-friendly interactive maps. (v.1.9.4) [Software Library]. https://github.com/Leaflet/Leaflet

Alabbad, Y., Mount, J., Campbell, A. M., & Demir, I. (2024). A web-based decision support framework for optimizing road network accessibility and emergency facility allocation during flooding. Urban Informatics, 3(1). https://doi.org/10.1007/s44212-024-00040-0

Alabbad, Y., Yildirim, E., & Demir, I. (2023). A web-based analytical urban flood damage and loss estimation framework. Environmental Modelling & Software, 163, 105670. https://doi.org/10.1016/j.envsoft.2023.105670

Aristizabal, F., Chegini, T., Petrochenkov, G., Salas, F., & Judge, J. (2024). Effects of high-quality elevation data and explanatory variables on the accuracy of flood Inundation mapping via height above nearest drainage. Hydrology and Earth System Sciences, 28(6), 1287-1315. https://doi.org/10.5194/hess-28-1287-2024

Aristizabal, F., Salas, F., Petrochenkov, G., Grout, T., Avant, B., Bates, B., Spies, R., Chadwick, N., Wills, Z., & Judge, J. (2023). Extending height above nearest drainage to model multiple fluvial sources in flood Inundation mapping applications for the U.S. national water model. Water Resources Research, 59(5). https://doi.org/10.1029/2022wr032039

Baruah, A., Dhital, S., Cohen, S., Duc Tran, T. N., Elhaddad, H., Watts, C. L., Devi, D., Chen, Y., & Pruitt, C. (2025a). FIMserv v.1.0: A tool for streamlining flood Inundation mapping (FIM) using the United States operational hydrological forecasting framework. Environmental Modelling & Software, 192, 106581. https://doi.org/10.1016/j.envsoft.2025.106581

Baruah, A., Spies, R., Devi, D., Cohen, S., Aristizabal, F., Nikrou, P., Tian, D., & Pruitt, C. (2025b). Predicting synthetic rating curve adjustment factors with explainable machine learning for enhancing the United States operational flood Inundation mapping framework. Journal of Hydrology, 662, 134086. https://doi.org/10.1016/j.jhydrol.2025.134086

Bertsch, R., Glenis, V., & Kilsby, C. (2022). Building level flood exposure analysis using a hydrodynamic model. Environmental Modelling & Software, 156, 105490. https://doi.org/10.1016/j.envsoft.2022.105490

Blodgett, D., & Johnson, M. (2025). Progress toward a reference hydrologic Geospatial fabric for the United States. Water Data For The Nation Blog. https://waterdata.usgs.gov/blog/hydrofabric/

Brakebill, J. W., Schwarz, G. E., & Wieczorek, M. E. (2020). An enhanced hydrologic stream network based on the NHDPlus medium resolution dataset. Scientific Investigations Report. https://doi.org/10.3133/sir20195127

CARTO. (2024). Basemaps. CARTO Documentation. https://docs.carto.com/carto-user-manual/maps/basemaps

Cikmaz, B. A., Yildirim, E., & Demir, I. (2023). Flood susceptibility mapping using fuzzy analytical hierarchy process for cedar rapids, Iowa. International Journal of River Basin Management, 23(1), 1-13. https://doi.org/10.1080/15715124.2023.2216936

Cosgrove, B., Gochis, D., Flowers, T., Dugger, A., Ogden, F., Graziano, T., Clark, E., Cabell, R., Casiday, N., Cui, Z., Eicher, K., Fall, G., Feng, X., Fitzgerald, K., Frazier, N., George, C., Gibbs, R., Hernandez, L., Johnson, D., … Zhang, Y. (2024). NOAA's national water model: Advancing operational hydrology through continental-scale modeling. JAWRA Journal of the American Water Resources Association, 60(2), 247-272. https://doi.org/10.1111/1752-1688.13184

Costabile, P., Lombardo, M., Costanzo, C., Tsoukalas, I., & Bellos, V. (2026). A stochastic rain-on-grid framework for handling spatio-temporal rainfall uncertainty in impact-based flood nowcasting. International Journal of Disaster Risk Reduction, 134, 105998. https://doi.org/10.1016/j.ijdrr.2026.105998

Dazzi, S., Vacondio, R., & Mignosa, P. (2019). Integration of a levee breach erosion model in a GPU-accelerated 2D shallow water equations code. Water Resources Research, 55(1), 682-702. https://doi.org/10.1029/2018wr023826

Demir, I., & Krajewski, W. F. (2013). Towards an integrated flood information system: Centralized data access, analysis, and visualization. Environmental Modelling & Software, 50, 77-84. https://doi.org/10.1016/j.envsoft.2013.08.009

Demiray, B. Z., Sermet, Y., Yildirim, E., & Demir, I. (2025). FloodGame: An interactive 3D serious game on flood mitigation for disaster awareness and education. Environmental Modelling & Software, 188, 106418. https://doi.org/10.1016/j.envsoft.2025.106418

DeVries, B., Huang, C., Armston, J., Huang, W., Jones, J. W., & Lang, M. W. (2020). Rapid and robust monitoring of flood events using Sentinel-1 and Landsat data on the Google Earth

engine. Remote Sensing of Environment, 240, 111664. https://doi.org/10.1016/j.rse.2020.111664

Dohler, D. (2022). Loam: JavaScript wrapper for GDAL in the browser. (v.1.2.0) [Software Library]. https://github.com/azavea/loam

Earth Resources Observation and Science (EROS) Center. (2022). Landsat Level-3 Dynamic Surface Water Extent, Collection 2 [Dataset]. U.S. Geological Survey. https://doi.org/10.5066/P9DPWBUS

Emiroglu, E., Grant, C. A., Sermet, Y., & Demir, I. (2025). Floodcraft: Game-based interactive learning environment using Minecraft for flood mitigation for K-12 education. International Journal of Disaster Risk Reduction, 130, 105799. https://doi.org/10.1016/j.ijdrr.2025.105799

Erazo Ramirez, C., Sermet, Y., Molkenthin, F., & Demir, I. (2022). HydroLang: An open-source web-based programming framework for hydrological sciences. Environmental Modelling & Software, 157, 105525. https://doi.org/10.1016/j.envsoft.2022.105525

Erazo Ramirez, C., Sermet, Y., & Demir, I. (2023). HydroLang markup language: Community-driven web components for hydrological analyses. Journal of Hydroinformatics, 25(4), 1171-1187. https://doi.org/10.2166/hydro.2023.149

Ewing, G., Mantilla, R., Krajewski, W., & Demir, I. (2022). Interactive hydrological modelling and simulation on client-side web systems: An educational case study. Journal of Hydroinformatics, 24(6), 1194-1206. https://doi.org/10.2166/hydro.2022.061

Gesch, D., Oimoen, M., Greenlee, S., Nelson, C., Steuck, M., & Tyler, D. (2002). The national elevation dataset. Photogrammetric engineering and remote sensing, 68(1), 5-32.

Gorelick, N., Hancher, M., Dixon, M., Ilyushchenko, S., Thau, D., & Moore, R. (2017). Google Earth engine: Planetary-scale geospatial analysis for everyone. Remote Sensing of Environment, 202, 18-27. https://doi.org/10.1016/j.rse.2017.06.031

Hales, R. C., Nelson, E. J., Souffront, M., Gutierrez, A. L., Prudhomme, C., Kopp, S., Ames, D. P., Williams, G. P., & Jones, N. L. (2022). Advancing global hydrologic modeling with the GEOGloWS ECMWF streamflow service. Journal of Flood Risk Management, 18(1). https://doi.org/10.1111/jfr3.12859

Horsburgh, J. S., Morsy, M. M., Castronova, A. M., Goodall, J. L., Gan, T., Yi, H., Stealey, M. J., & Tarboton, D. G. (2015). HydroShare: Sharing diverse environmental data types and models as social objects with application to the hydrology domain. JAWRA Journal of the American Water Resources Association, 52(4), 873-889. https://doi.org/10.1111/1752-1688.12363

Hu, A., & Demir, I. (2021). Real-time flood mapping on client-side web systems using HAND model. Hydrology, 8(2), 65. https://doi.org/10.3390/hydrology8020065

IPCC (Intergovernmental Panel on Climate Change). (2023). Technical summary. Climate Change 2021 – The Physical Science Basis, 35-144. https://doi.org/10.1017/9781009157896.002

Johnson, J. M., Munasinghe, D., Eyelade, D., & Cohen, S. (2019). An integrated evaluation of the national water model (nwm)–height above nearest drainage (HAND) flood mapping methodology. Natural Hazards and Earth System Sciences, 19(11), 2405-2420. https://doi.org/10.5194/nhess-19-2405-2019

Jones, K. A., Niknami, L. S., Buto, S. G., & Decker, D. (2009). Federal standards and procedures for the national watershed boundary dataset (WBD). Techniques and Methods. https://doi.org/10.3133/tm11a3

Kraft, L. L., Villarini, G., & Czajkowski, J. (2023). Characterizing the 2019 Midwest flood: A hydrologic and socioeconomic perspective. Weather, Climate, and Society, 15(3), 603-617. https://doi.org/10.1175/wcas-d-22-0065.1

Lazzarin, T., Viero, D. P., Molinari, D., Ballio, F., & Defina, A. (2022). Flood damage functions based on a single physics- and data-based impact parameter that jointly accounts for water depth and velocity. Journal of Hydrology, 607, 127485. https://doi.org/10.1016/j.jhydrol.2022.127485

Li, Z., & Demir, I. (2022). A comprehensive web-based system for flood Inundation map generation and comparative analysis based on height above nearest drainage. Science of The Total Environment, 828, 154420. https://doi.org/10.1016/j.scitotenv.2022.154420

Li, Z., Duque, F. Q., Grout, T., Bates, B., & Demir, I. (2023). Comparative analysis of performance and mechanisms of flood Inundation map generation using height above nearest drainage. Environmental Modelling & Software, 159, 105565. https://doi.org/10.1016/j.envsoft.2022.105565

McCallum, B. E., & Riskin, M. L. (2025). The U.S. geological survey national Streamgage network, 2024. General Information Product. https://doi.org/10.3133/gip252

Miller, J. (2025). Preact: Fast 3kB alternative to React with the same modern API. (v.10.27.1) [Software Library]. https://github.com/preactjs/preact

Moore, R. B., McKay, L. D., Rea, A. H., Bondelid, T. R., Price, C. V., Dewald, T. G., & Johnston, C. M. (2019). User's guide for the national hydrography dataset plus (NHDPlus) high resolution. Open-File Report. https://doi.org/10.3133/ofr20191096

Mostafiz, R. B., Friedland, C. J., Rahman, M. A., Rohli, R. V., Tate, E., Bushra, N., & Taghinezhad, A. (2021). Comparison of neighborhood-scale, residential property flood-loss assessment methodologies. Frontiers in Environmental Science, 9. https://doi.org/10.3389/fenvs.2021.734294

NASA Science. (2019a, March 18). Historic floods inundate Nebraska. NASA Earth Observatory. https://earthobservatory.nasa.gov/images/144691/historic-floods-inundate-nebraska

NASA Science. (2019b, March 19). Icy floodwaters grind through Iowa. NASA Earth Observatory. https://earthobservatory.nasa.gov/images/144696/icy-floodwaters-grind-through-iowa

National Water Prediction Service. (n.d.). National Water Prediction Service - NOAA. https://water.noaa.gov

Nelson, E. J., Pulla, S. T., Matin, M. A., Shakya, K., Jones, N., Ames, D. P., Ellenburg, W. L., Markert, K. N., David, C. H., Zaitchik, B. F., Gatlin, P., & Hales, R. (2019). Enabling stakeholder decision-making with earth observation and modeling data using Tethys platform. Frontiers in Environmental Science, 7. https://doi.org/10.3389/fenvs.2019.00148

NOAA Office of Water Prediction. (2025). Inundation Mapping. GitHub. https://github.com/NOAA-OWP/inundation-mapping

Nobre, A., Cuartas, L., Hodnett, M., Rennó, C., Rodrigues, G., Silveira, A., Waterloo, M., & Saleska, S. (2011). Height above the nearest drainage – a hydrologically relevant new terrain model. Journal of Hydrology, 404(1-2), 13-29. https://doi.org/10.1016/j.jhydrol.2011.03.051

Qian, Q., Edwards, D. J., Zhang, Y., & Haselbach, L. (2024). Improving flood Inundation mapping accuracy using HEC-RAS modeling: A case study of the Neches river tidal floodplain in Texas. Journal of Hydrologic Engineering, 29(4). https://doi.org/10.1061/jhyeff.heeng-6037

Ramirez, C. E., Sermet, Y., & Demir, I. (2024). HydroCompute: An open-source web-based computational library for hydrology and environmental sciences. Environmental Modelling & Software, 175, 106005. https://doi.org/10.1016/j.envsoft.2024.106005

Rebolho, C., Andréassian, V., & Le Moine, N. (2018). Inundation mapping based on reach-scale effective geometry. Hydrology and Earth System Sciences, 22(11), 5967-5985. https://doi.org/10.5194/hess-22-5967-2018

Sabaren, L. N., Mascheroni, M. A., Greiner, C. L., & Irrazábal, E. (2018). A systematic literature review in cross-browser testing. Journal of Computer Science and Technology, 18(01), e03. https://doi.org/10.24215/16666038.18.e03

Samela, C., Albano, R., Sole, A., & Manfreda, S. (2018). A GIS tool for cost-effective delineation of flood-prone areas. Computers, Environment and Urban Systems, 70, 43-52. https://doi.org/10.1016/j.compenvurbsys.2018.01.013

Scawthorn, C., Flores, P., Blais, N., Seligson, H., Tate, E., Chang, S., Mifflin, E., Thomas, W., Murphy, J., Jones, C., & Lawrence, M. (2006). HAZUS-MH flood loss estimation methodology. II. Damage and loss assessment. Natural Hazards Review, 7(2), 72-81. https://doi.org/10.1061/(asce)1527-6988(2006)7:2(72)

Seneviratne, S. I., Zhang, X., Adnan, M., Badi, W., Dereczynski, C., Luca, A. D., Ghosh, S., Iskandar, I., Kossin, J., Lewis, S., Otto, F., Pinto, I., Satoh, M., Vicente-Serrano, S. M., Wehner, M., Zhou, B., & Allan, R. (2021). Weather and climate extreme events in a changing climate. Climate Change 2021: The Physical Science Basis: Working Group I contribution to the Sixth Assessment Report of the Intergovernmental Panel on Climate Change, 1513-1766. https://doi.org/10.1017/9781009157896.013

Sit, M., Langel, R. J., Thompson, D., Cwiertny, D. M., & Demir, I. (2021). Web-based data analytics framework for well forecasting and groundwater quality. *Science of The Total Environment*, *761*, 144121. https://doi.org/10.1016/j.scitotenv.2020.144121

Sit, M., Sermet, Y., & Demir, I. (2019). Optimized watershed delineation library for server-side and client-side web applications. Open Geospatial Data, Software and Standards, 4(1). https://doi.org/10.1186/s40965-019-0068-9

Sufi, M., Ramirez, C. E., & Demir, I. (2025). HydroLang FRAM: Web-based framework for comprehensive flood risk and mitigation assessment and communication. International Journal of Disaster Risk Reduction, 128, 105735. https://doi.org/10.1016/j.ijdrr.2025.105735

Sugarbaker, L. J., Constance, E. W., Heidemann, H. K., Jason, A. L., Lukas, V., Saghy, D. L., & Stoker, J. M. (2014). The 3D elevation program initiative: A call for action. Circular. https://doi.org/10.3133/cir1399

Teng, J., Jakeman, A., Vaze, J., Croke, B., Dutta, D., & Kim, S. (2017). Flood Inundation modelling: A review of methods, recent advances and uncertainty analysis. Environmental Modelling & Software, 90, 201-216. https://doi.org/10.1016/j.envsoft.2017.01.006

Thalakkottukara, N. T., Thomas, J., Watkins, M. K., Holland, B. C., Oommen, T., & Grover, H. (2024). Suitability of the height above nearest drainage (HAND) model for flood Inundation mapping in data-scarce regions: A comparative analysis with hydrodynamic models. Earth Science Informatics, 17(3), 1907-1921. https://doi.org/10.1007/s12145-023-01218-x

Tomkins, K. M. (2012). Uncertainty in streamflow rating curves: Methods, controls and consequences. Hydrological Processes, 28(3), 464-481. https://doi.org/10.1002/hyp.9567

Townsend, J. T. (1971). Theoretical analysis of an alphabetic confusion matrix. Perception & Psychophysics, 9(1), 40-50. https://doi.org/10.3758/bf03213026

Trenberth, K. E., Fasullo, J. T., & Shepherd, T. G. (2015). Attribution of climate extreme events. Nature Climate Change, 5(8), 725-730. https://doi.org/10.1038/nclimate2657

Tsegaye, S., Kebedew, M. G., Albrecht, K. K., Missimer, T. M., Thomas, S., & Elshall, A. S. (2024). Integrated GIS-hydrologic-hydraulic modeling to assess combined flood drivers in coastal regions: A case study of Bonita Bay, Florida. Frontiers in Water, 6. https://doi.org/10.3389/frwa.2024.1468354

U.S. Army Corps of Engineers. (2022). National Structure Inventory: Technical documentation. Hydrologic Engineering Center. https://www.hec.usace.army.mil/confluence/nsi/technicalreferences/latest/technical-documentation

Velásquez, N., Quintero, F., Koya, S. R., Roy, T., & Mantilla, R. (2023). Snow-detonated floods: Assessment of the U.S. Midwest March 2019 event. Journal of Hydrology: Regional Studies, 47, 101387. https://doi.org/10.1016/j.ejrh.2023.101387

Wang, Y. (2025). Towards more efficient urban flood assessment: Issue of spatial resolution in urban flood hydrodynamic modeling from flood exposure perspective. Water Resources Management, 39(12), 6683-6700. https://doi.org/10.1007/s11269-025-04267-7

Wathan, A. (2024). Tailwind CSS: A utility-first CSS framework for rapid UI development. (v.3.4.17) [Software Library]. https://github.com/tailwindlabs/tailwindcss

Wing, O. E., Bates, P. D., Smith, A. M., Sampson, C. C., Johnson, K. A., Fargione, J., & Morefield, P. (2018). Estimates of present and future flood risk in the conterminous United States. Environmental Research Letters, 13(3), 034023. https://doi.org/10.1088/1748-9326/aaac65

Xing, Y., Shao, D., Lin, Q., Ullah, I., Wang, J., & Wang, Y. (2025). Towards more efficient urban flood assessment: Issue of spatial resolution in urban flood hydrodynamic modeling from flood exposure perspective. Water Resources Management, 39(12), 6683-6700. https://doi.org/10.1007/s11269-025-04267-7

You, E. (2025). Vite: Next generation frontend tooling. (v.6.3.5) [Software Library]. https://github.com/vitejs/vite